

Delta production by pion charge exchange on complex nuclei

B. L. Clausen, R. A. Loveman, R. J. Peterson, R. A. Ristinen, and J. L. Ullmann*
Nuclear Physics Laboratory, University of Colorado, Boulder, Colorado 80309

F. Irom

Los Alamos National Laboratory, Los Alamos, New Mexico 87545

(Received 6 October 1986)

We have used the (π^-, π^0) reaction at a beam energy of 475 MeV on targets of ^1H , ^2H , C, and ^{90}Zr to examine excitations near 300 MeV. At this excitation energy, delta production is expected to occur by charge exchange on a nucleon. Our (π^-, π^0) results for delta production in complex nuclei are compared to those for photoabsorption, (p,n), and $(^3\text{He}, t)$ reactions. The target mass dependence of the absorption for the three charge-exchange reactions is found to be similar.

I. INTRODUCTION

The $(^3\text{He}, t)$ (Refs. 1–4) and (p,n) (Refs. 5–9) charge-exchange reactions on complex nuclei display a broad, prominent peak at an excitation of 300 MeV. Due to its similarity in excitation and width to free delta-particle production, this feature is interpreted as a delta particle (resulting from a spin-isospin excitation of the nucleon to the $T = \frac{3}{2}$, $J = \frac{3}{2}$, 3-3 or delta isobar). The present experiment uses another single-charge-exchange reaction, (π^-, π^0) , to study this delta-excitation region in complex nuclei to complement the baryonic experiments. The five possible diagrams for a π^- incident on a nucleon to form a delta particle and also a π^0 are shown in Fig. 1, along with a generalized diagram for labeling purposes. The first vertex might occur, for instance, through ρ exchange. Note that both an “extra” π^0 (variously called a direct π^0 or spectator π^0) and a “decay” π^0 may be produced. The generalized diagram is similar to that used previously for analyses of (p,n) and $(^3\text{He}, t)$ data.¹⁰

The (π^\pm, π^0) reaction gives new information not available from nucleon-induced charge exchange. For the spin-zero pion the spin transfer must be transverse, while a longitudinal excitation is permitted for protons or ^3He . Thus, if in fact the charge exchange is to a delta particle, the “extra” (π, π^0) cross section must vanish at zero degrees. This could give an added confirmation that the observed bump is a delta particle, or serve to separate “extra” and “decay” contributions. Another advantage is that (π^+, π^0) and (π^-, π^0) charge-exchange reactions can be easily compared, unlike nuclear charge-exchange reactions. Recent excitations of delta states by heavy ion beams have compared both directions for charge exchange,¹¹ but these results cannot be compared in detail since the final ejectiles contain different arrays of bound states.

II. THE EXPERIMENT

The (π^-, π^0) experiment was performed at the Clinton P. Anderson Los Alamos Meson Physics Facility (LAMPF) using the high-energy pion beam line (P^3) with

a π^- beam energy of 475 MeV ($k = 3.0 \text{ fm}^{-1}$). The pion flux used was 1×10^6 to 2×10^6 pions per second with $\Delta p/p$ (the momentum acceptance of the beam as set by the channel slits) ranging from 0.5% to 0.8%. This flux was periodically determined by ^{11}C activation measurements, using the cross sections of Butler *et al.*,¹² and was checked during the runs by counting beam particles with a sampling grid scintillator two meters downstream from the target. The agreement between these two methods was within 5%.

Four targets were used with several areal densities: CH_2 (0.3–1.7 g/cm²), CD_2 (0.7–1.1 g/cm²), C (0.5–3.1 g/cm²), and ^{90}Zr enriched to 97.7% (1.8 g/cm²). In all cases the measured cross section was found to be independent of target thickness, ruling out a contribution from multiple π^- scattering in the thick targets used.

The π^0 s were detected using the LAMPF π^0 spectrometer that has been described in detail elsewhere.^{13,14} The spectrometer was used in the “two-post” configuration, where the scattering angle is in the vertical plane. The first converter in each detector arm was set 90 cm from the target. The detection crates were centered at a scattering angle of 25° and actually detected π^0 s between about 10° and 40°. The crates were set at three different opening angles to look at three overlapping regions of the π^0 energy spectrum with acceptance peaks centered at 70, 130, and 190 MeV. This gives π^- laboratory energy losses of 405, 345, and 285 MeV, respectively, to cover the expected delta region found in $(^3\text{He}, t)$ and (p,n) reactions. The requirements on opening angle and total energy select two photons from a single π^0 , and discriminate against uncorrelated photons from two π^0 s, as from reaction 1 in Fig. 1.

A π^- beam was used for the present work in order to avoid the proton contamination that would accompany a π^+ beam. The isospin change of the targets is thus opposite to that induced by (p,n) and $(^3\text{He}, t)$ reactions, but comparable to that for the (n,p) or (d,2p) reactions. The angle chosen for the present study is based upon an expected zero cross section at zero degrees for the “extra” π^0 and a rapid decrease at larger angles due to the large

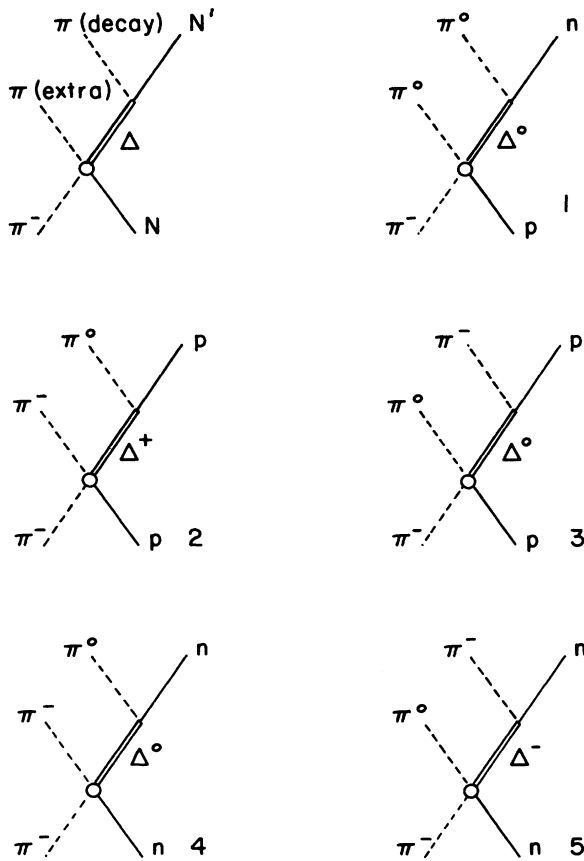


FIG. 1. Possible reaction diagrams for a π^- incident upon a nucleon to form a delta particle and either an "extra" or a "decay" π^0 .

momentum transfer to the high-lying state. In an eikonal model,¹⁵ the cross section for the "extra" π^0 depends upon θ and q as

$$\frac{d\sigma}{d\Omega} \propto \sin^2\theta \frac{e^{-2\pi a q}}{q^2}.$$

With $a = 0.50$ fm as a typical nuclear diffuseness, this cross section is maximum near 25° . Delta-particle production by pions on hydrogen has much this expected dependence.¹⁶

The "decay" π^0 need not follow this angular dependence, and direct production of nucleonic excitations of spin $\frac{1}{2}$, not requiring a spin excitation, also need not agree with this expectation. A complete angular distribution could distinguish these options for the origin of the π^0 's, but was not available in the present experiment.

III. DATA ANALYSIS

During analysis of the data the software constraints were set liberally to gain the most events over a broad energy acceptance. The energy from π^0 decay is shared between two decay photons. For the present work the energy sharing parameter $X = (E_1 - E_2)/(E_1 + E_2)$ was limited to 0.4 or less. One possible inaccuracy in determining

the photon energy is related to the fraction of the charged particle shower contained in the lead-glass block calorimeter. A minimum value of 3 radiation lengths was used to determine positions for photon conversion in the conversion planes that gave acceptable containment in the calorimeter. These software constraints gave an energy resolution ranging from 6 MeV at the low end of the energy spectrum to 13 MeV at the high end of the energy spectrum.

The data were divided by software into three laboratory scattering angle bins: 0° – 22° , 22° – 28° , and 28° – 50° . From Monte Carlo simulations the average angles for the bins were 18° , 25° , and 33° , respectively, with an overall average of 27° . Variances for the angular resolution for each bin were also computed from the Monte Carlo simulation, and data are plotted with these uncertainties.

The spectrometer solid angle used for cross-section calculations was found using a Monte Carlo simulation, with the results for the three spectrometer settings shown in Fig. 2. In combining data from the three spectrometer settings the 45–100 MeV spectra were taken from the 70-MeV setting, the 100–160 MeV spectra were taken from the 130-MeV setting, and the 160–400 MeV spectra were taken from the 190-MeV setting. As can be seen in Fig. 2, there is some overlap between spectrometer settings. Before combining the spectra, it was noted that the spectra matched well in this overlap region, except for Zr.

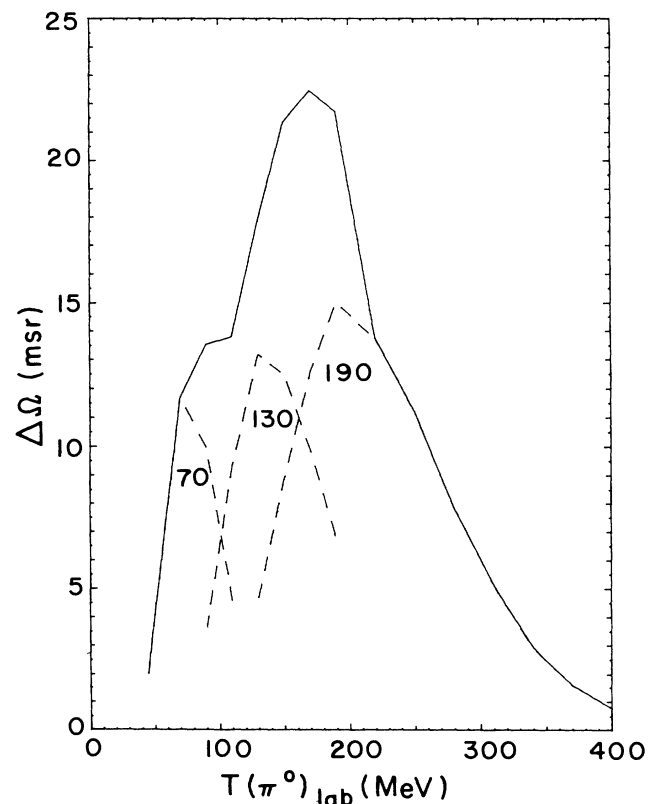


FIG. 2. The π^0 -spectrometer acceptance as calculated from a Monte Carlo simulation. The spectrometer solid angle is given as a function of π^0 energy for the three spectrometer settings used.

In that case the normalized spectrum of the 70-MeV setting was about 20% higher than that for the 130-MeV setting where they overlapped, although the two spectra did match within the error bars. We note that at 400 MeV the solid angle is down to 5% of the 190-MeV maximum. It is questionable how well the Monte Carlo simulation models the spectrometer acceptance below 20%, so the accuracy of the spectra between π^0 energies of 340 and 400 MeV is uncertain.

As a check on detector efficiencies, data were taken on the $p(\pi^-, \pi^0)n$ reaction with 165 MeV π^- and the spectrometer at the 190-MeV setting. The ray tracing efficiency, E_{rt} , was adjusted to give cross sections in agreement with the cross sections computed from the SP86 phase shifts.¹⁷ We conclude that the normalization is accurate to within $\pm 9\%$.

The raw data histograms were adjusted as follows: (1) the several runs for each spectrometer setting and target were added; (2) data for the empty target frame were subtracted (this amounted to subtracting about 15% of the raw data); (3) the histograms were corrected for spectrometer acceptance as computed by the Monte Carlo simulation; (4) the histograms were normalized based on pion flux, efficiencies, and target thickness; (5) the three spec-

trometer settings were combined; and (6) carbon events were subtracted from CH_2 and CD_2 . (About two thirds of the error bars for the ^1H and ^2H spectra are from this C subtraction.)

Cross sections were calculated using

$$\frac{d^2\sigma}{d\Omega dE} = \frac{Y}{\phi N_t} \frac{1}{\Delta\Omega_{MC}} \frac{1}{\Delta E} \frac{1}{\tau A E_{jk} E_{mwpc} E_{rt}},$$

where Y is the yield, ϕ is the pion flux, N_t is the number of target nuclei per cm^2 , $\Delta\Omega_{MC}$ is the Monte Carlo calculated solid angle, ΔE is the size of the energy bin (10 MeV), τ is the computer live time (76–96%), A corrects for the decay-photon attenuation in the target and detectors (83–92%), E_{jk} is the joint detection efficiency in the two spectrometer arms (29% at low energies to 45% at high energies as calculated using the equations of Ref. 14), E_{mwpc} is the wire-chamber efficiency (66–84%), and E_{rt} is the ray tracing efficiency [80% based on normalization to the $p(\pi^-, \pi^0)n$ reaction]. It should be noted that E_{rt} was 90% when the energy-sharing parameter, X , was limited to 0.3, as is more standard when data at low excitations are analyzed and higher resolution is necessary.

IV. RESULTS

The laboratory frame π^0 spectra from ^1H , ^2H , C, and ^{90}Zr for the three angle bins separately are shown in Figs.

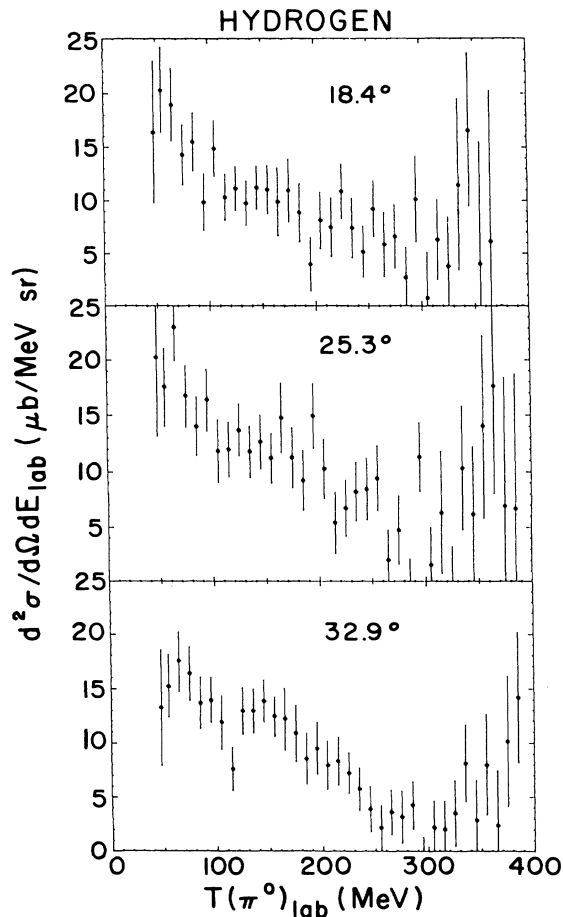


FIG. 3. Laboratory π^0 energy spectra from hydrogen for the three angle bins.

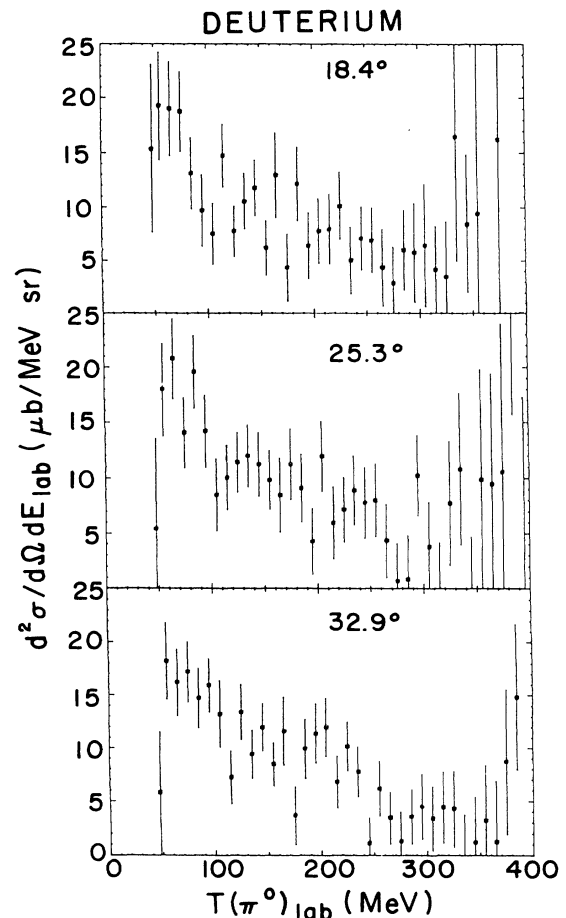


FIG. 4. Laboratory π^0 energy spectra from deuterium for the three angle bins.

3–6 with the spectra for each target summed over the angle bins shown in Fig. 7. The π^0 's in the spectra between about 100 and 300 MeV are expected to be mainly due to delta production, whether we use the kinematics for quasifree scattering to a delta particle or the kinematics for excitation of a bound delta-hole state. Using free proton kinematics for quasifree scattering, the “extra” π^0 centroid is at 116 MeV and the maximum “extra” π^0 energy is 305 MeV. Using mass 90 kinematics for producing a bound delta-hole state in ^{90}Zr , the “extra” π^0 centroid is at 186 MeV and the maximum “extra” π^0 energy is 344 MeV. (The “extra” π^0 maximum energy occurs when the delta has a minimum mass of 1074 MeV—the sum of the masses of its decay products.) It is found that the “decay” π^0 energy is also in the 100–300 MeV range for either kinematic assumption.

The π^0 's below 100 MeV and above 300 MeV must be due mainly to some source other than delta production. We therefore look at some other possible sources of π^0 's. As mentioned above, the Monte Carlo modeling is uncertain above about 340 MeV, so the actual number of π^0 's at the high end of the energy spectrum is questionable. A possible source of π^0 's in the high energy region is from

quasifree nucleon scattering, without delta excitation. For the scattering angle we are looking at, the π^0 's would have a mean energy as low as 420 MeV, and the tail of this broad quasifree peak would enter our spectra.

Another possible source of π^0 's is the (π^-, π^0) production of an $N^*(1440)$ instead of a delta particle. At the low energy end of our spectra the edge of the broad peak for the “extra” π^0 produced in this reaction will appear with the half-maximum position of the peak occurring at about 100 MeV. For these low energy events there is also a kinematic compression. For inclusive π^- scattering at 5 GeV a complete inelastic spectrum is shown in Fig. 7 of Ref. 18. The overlap of the broad delta (1232 MeV) and $N^*(1440)$ peaks is clear, with the strength of the latter such that many low energy π^0 events would be anticipated in our spectra. At the high energy end of our spectra a “decay” π^0 can be produced from the $N^*(1440)$ with the energy centroid larger than 400 MeV and the half-maximum position of the peak occurring at about 215 MeV. $N^*(1440)$ production could thus contribute π^0 's at both the low and high energy end of our spectra.

In analyzing the π^0 spectrum between 100 and 300 MeV, we have assumed quasifree scattering to the delta

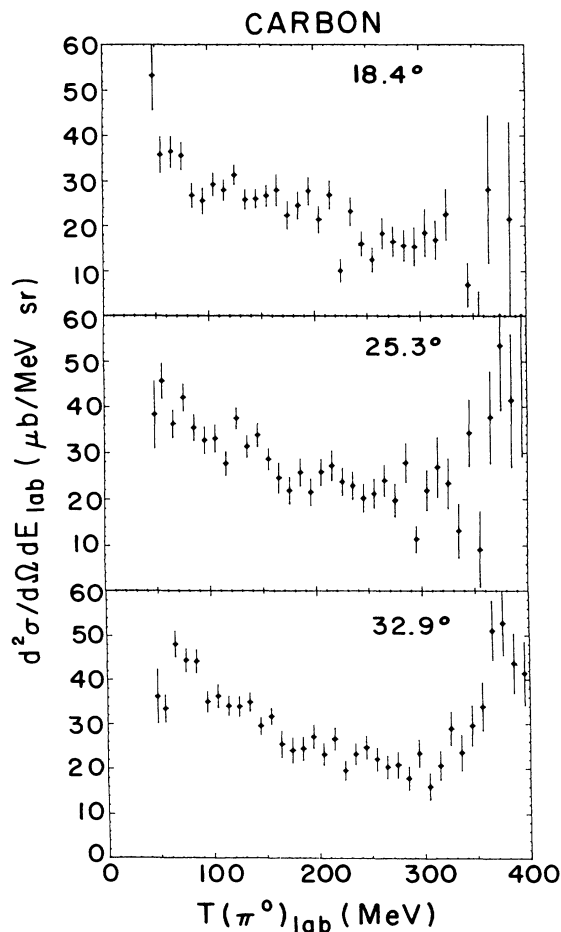


FIG. 5. Laboratory π^0 energy spectra from carbon for the three angle bins.

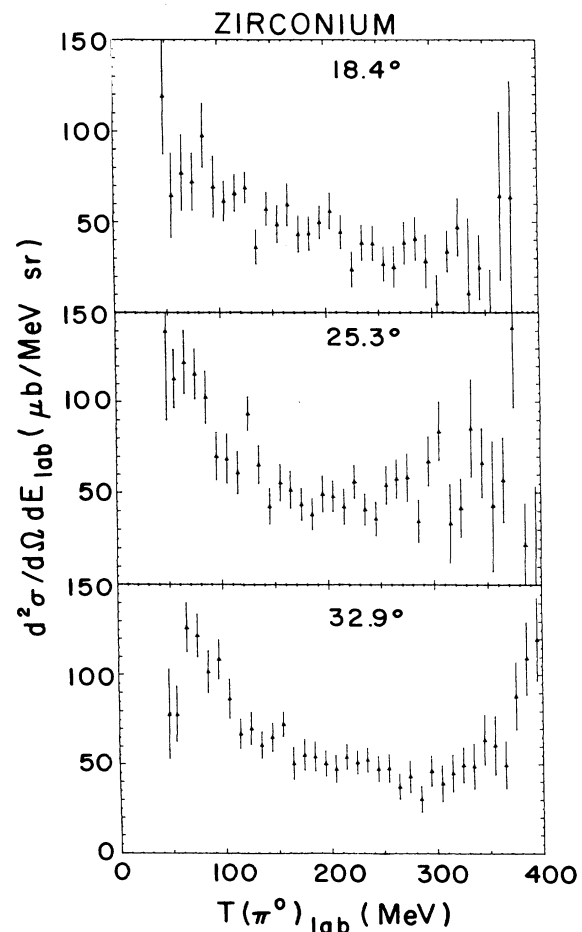


FIG. 6. Laboratory π^0 energy spectra from ^{90}Zr for the three angle bins.

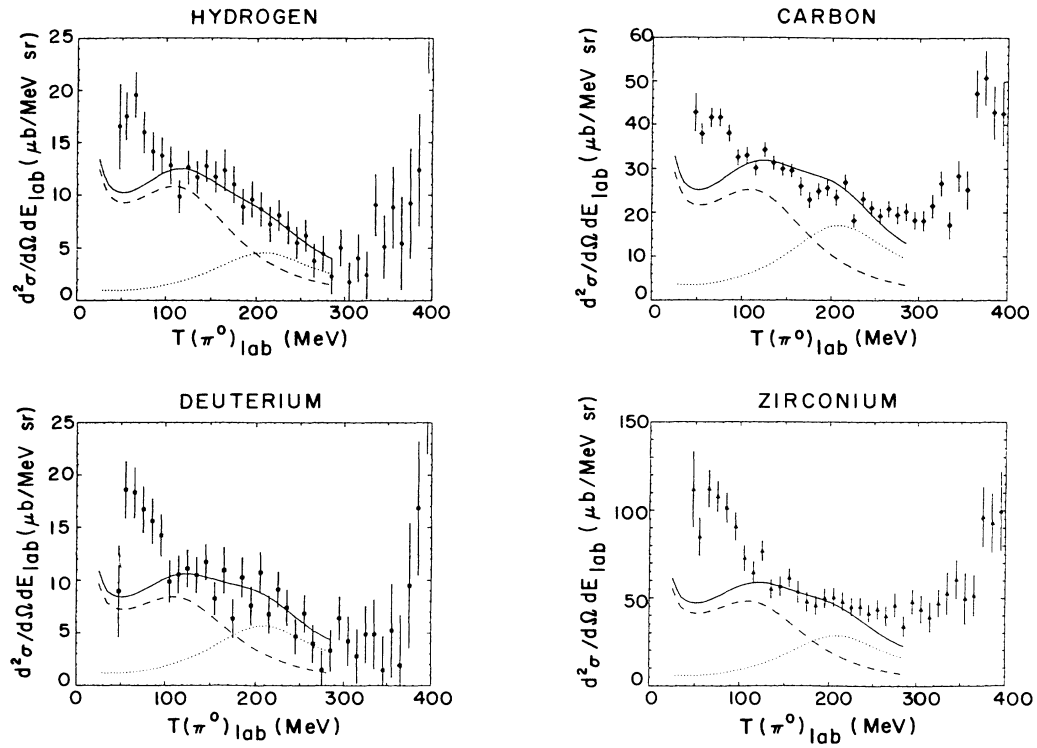


FIG. 7. Laboratory π^0 energy spectra summed over the three angle bins (for an average angle of 27°). A peak shape (solid line) is fit to the data using the sum of an “extra” π^0 peak (dashed line) and a “decay” π^0 peak (dotted line). The resulting cross sections are given in Table I.

TABLE I. Laboratory differential cross sections (in mb/sr) for the (π^-, π^0) reaction at 475 MeV are listed. They were calculated from the spectra of Fig. 7. The “extra” and “decay” cross sections result from integrating the fitted peaks in Fig. 7 between 25 and 290 MeV and the “fit” cross section is the sum of these two. The “data” cross section results from summing the data between 45 and 300 MeV. The “fit” cross sections have an uncertainty of 20%. $\bar{A} = 3N + Z$ for these reactions.

	\bar{A}	Region	$\frac{d\sigma}{d\Omega}$	$\left(\frac{d\sigma}{d\Omega}\right) / \bar{A}$
Hydrogen	1	“extra”	1.91	1.9
		“decay”	0.71	0.71
		“fit”	2.62	
		“data”	2.60	2.6
Deuterium	4	“extra”	1.49	0.37
		“decay”	0.88	0.22
		“fit”	2.37	
		“data”	2.46	0.61
Carbon	24	“extra”	4.46	0.19
		“decay”	2.66	0.11
		“fit”	7.12	
		“data”	7.10	0.30
Zirconium	190	“extra”	8.50	0.045
		“decay”	4.43	0.023
		“fit”	12.9	
		“data”	15.8	0.083

TABLE II. Laboratory "data" differential cross sections (in mb/sr) for the energy spectra in Figs. 3–6 obtained by summing the data between 45 and 300 MeV.

	$18^\circ \pm 4^\circ$	$25^\circ \pm 3^\circ$	$33^\circ \pm 4^\circ$
Hydrogen	2.62 ± 0.14	2.86 ± 0.14	2.41 ± 0.12
Deuterium	2.45 ± 0.17	2.51 ± 0.17	2.42 ± 0.14
Carbon	6.32 ± 0.16	7.20 ± 0.16	7.47 ± 0.13
Zirconium	13.3 ± 0.7	16.6 ± 0.6	16.6 ± 0.5

particle. For a laboratory scattering angle of 27° this results in a centroid at 116 MeV for the "extra" π^0 and 206 MeV for the "decay" π^0 . The laboratory widths of the π^0 peaks are 170 MeV and 155 MeV, respectively, corresponding to the free 120-MeV (center-of-mass) width for the delta particle as used in Ref. 10. Due to Fermi motion and Pauli blocking a width different from 120 MeV could be obtained for the C and Zr spectra, as in the detailed calculation of Ref. 10 for the ($^3\text{He},t$) spectra. We note that the two π^0 peaks could be separated by using a π^- beam with energy much larger than 475 MeV. For example, with a 760 MeV π^- beam the centroids for the "extra" and "decay" π^0 's in the laboratory frame would be 372 MeV and 222 MeV, respectively, and the half-maxima of the two peaks would no longer overlap. The spectra would then resemble those obtained by the high energy (p,n) and ($^3\text{He},t$) reactions. In Ref. 10, the existence of a decay neutron in the spectra for the (p,n) reaction was isolated, but not treated quantitatively.

If we had assumed the excitation of a bound delta-hole state instead of quasifree delta production, kinematics at a

scattering angle of 27° give the centroids of the "extra" and "decay" π^0 peaks, respectively, as 151 and 183 MeV for ^2H , 180 and 151 MeV for C, and 186 and 158 MeV for Zr. These peak separations are much smaller than for quasifree scattering (with hydrogen kinematics) and would be expected to give a more pronounced bump rather than the broad yield between 100 and 300 MeV that we in fact see.

Based on the above discussion, we fit the data in Fig. 7 between only 100 and 275 MeV with curves calculated for π^0 's from quasifree delta production. The curves are extended beyond this, but are not intended to fit the data. Several approximations were made in the peak fitting procedure. Since the kinematics of all five reactions in Fig. 1 are about the same, only the first reaction was used. The average value of 27° was used for the scattering angle of both the "extra" and the "decay" π^0 . The delta resonance was assumed to have a Lorentzian shape with a centroid of 1232 MeV and a width of 120 MeV in the center of mass. With these values the shape, centroid, and width of the two π^0 peaks are determined. The spectra were then fit by varying only the two peak heights (independently), with the results shown in Fig. 7.

The differential cross sections calculated for each target are listed in Table I. The "extra" π^0 and "decay" π^0 cross sections were found by integrating the fitted peaks in Fig. 7 between 25 and 290 MeV. The "fit" cross section is the sum of these two. The "data" cross section was found by summing the data between 45 and 300 MeV including events at the ends of the spectra not included in the fits. The assigned uncertainty of $\pm 20\%$ for the "fit" cross sections is made up of $\pm 9\%$ due to normalization and $\pm 18\%$ for the peak fitting.

"Data" differential cross sections were also found for the separate angle bins by summing the data between 45 and 300 MeV in Figs. 3–6. The results are listed in Table II and plotted in Fig. 8.

V. DISCUSSION

Theoretical studies of longitudinal excitation of delta-hole states on complex nuclei find two modes in the spin response, only one of which is observable in the timelike region ($\omega > q$).^{19–21} This peak is shifted lower in excitation for complex targets than is found for the free proton. Just this effect is found by experiment for ($^3\text{He},t$) reactions.^{1,10} For the transverse mode [as excited by (π, π^0)] only one delta-hole state is expected, shifted but little from the free delta excitation,^{19–21} but that shift is to higher excitations.¹⁹ Our data are inconclusive as to whether this shift is observable, due to overlapping peaks from the "extra" and the "decay" pions at the low beam

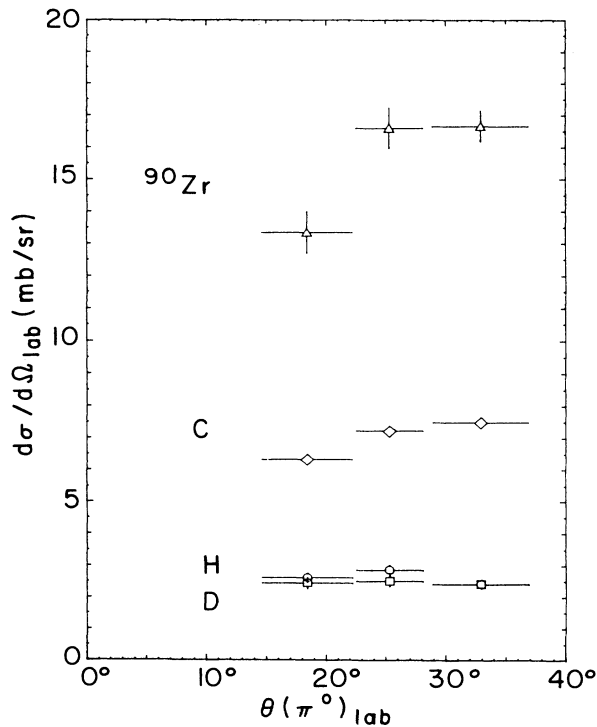


FIG. 8. Cross sections for the four targets as a function of angle obtained by summing the data in Figs. 3–6 between 45 and 300 MeV. The values plotted are listed in Table II.

energy used. Thus, we cannot use kinematic shifts to determine whether we are seeing a bound delta-hole state or quasifree scattering.

We compare our cross sections to the data compiled by Olsson and Yodh.²² In their Fig. 2 they show total inelastic cross sections for 475 MeV π^- on hydrogen summed over all angles as follows:

$$\pi^- + p \rightarrow \pi^0 + \pi^0 + n: 2.3 \text{ mb}$$

(our Fig. 1, the first reaction)

$$\pi^- + p \rightarrow \pi^- + \pi^0 + p: 1.6 \text{ mb}$$

(our Fig. 1, the second and third reactions). Their total cross section over all angles for producing one observed π^0 is 6.2 mb (2.3 + 2.3 + 1.6) for $\pi^- + p$. We integrate our differential cross sections for hydrogen in Fig. 8 over the small angular range of 14° – 37° to give a (partial) total laboratory cross section of 2.8 mb for the same reaction. Our cross section for the small angular range 14° – 37° is thus about half the cross section of Olsson and Yodh for all angles, so evidently our experiment was run near the maximum differential cross section.

From Ref. 22 the ratio of “extra” to “decay” π^0 s over all angles could be anywhere from $(2.3)/(2.3 + 1.6) = 0.6$ (using only the first and second reactions) to $(2.3 + 1.6)/(2.3) = 1.7$ (using only the first and third reactions). In our fits for hydrogen, this ratio is $1.91/0.71 = 2.69$. This comparison confirms that the “extra” pion yield is enhanced at our angle of observation.

Next we compare our results to data and calculations for photoabsorption, since the spin response for both pion charge exchange and for photoabsorption must be transverse. The photoabsorption data for targets from Li to U show very much the same cross section per nucleon, and the delta peak is broader and a bit weaker than found for photoabsorption on the proton.²³ These results are shown in Fig. 9, where they are compared to our pion charge-exchange data on ^1H , C, and ^{90}Zr from Fig. 7. Our data are converted from the laboratory frame to the center-of-mass frame (using quasifree delta-production kinematics) and plotted as a function of energy loss, ω . Since we are unable to separate the contributions of the two π^0 s in our data, we have approximated the π -N kinematics by using only the “extra” π^0 -N kinematics in the conversion for all targets. The angle selected for the experiment should select this “extra” π^0 .

Finally, we compare our pion absorption results with those from several other reactions, particularly $(^3\text{He}, t)$ and (p, n) . In the quark model, Suzuki and Kohn²⁴ have derived a sum rule for spin-isospin excitations of delta-hole states in the (π^-, π^0) reaction:

$$\sum_{\Delta, h} \langle \Delta | \sigma_i \tau_i | h \rangle^2 = \frac{128}{9} A \left[1 + \frac{N-Z}{2A} \right],$$

leading to an expectation of pion charge exchange (neglecting absorption) proportional to $\bar{A} = 3N + Z$. These weightings for neutron and proton contributions to the delta peak may also be obtained directly by application of the Wigner-Eckart theorem in isospin to a non-resonant reaction diagram, as in our Fig. 1, incoherently

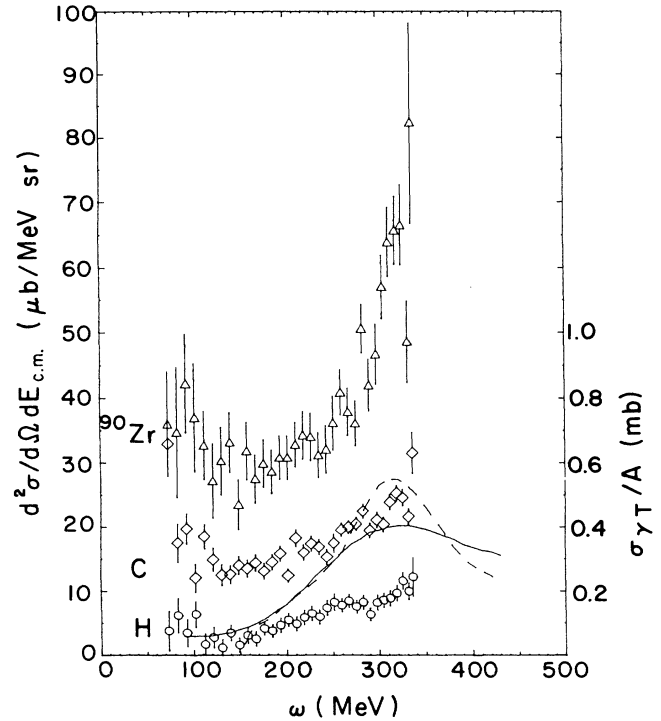


FIG. 9. The data of Fig. 7 replotted in the center-of-mass frame (assuming quasifree ^1H kinematics for all targets) as a function of energy loss. The lines are data from Ref. 23, Fig. 1 for the total photon absorption cross section per nucleon. The dashed line is for data from H and the solid line is for data from Li to U.

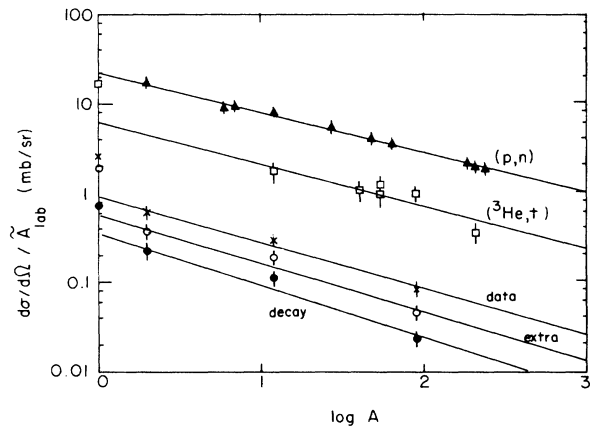


FIG. 10. Closed circles, open circles, and crosses show the 27° cross sections divided by $\bar{A} = Z + 3N$ for the $(\pi^-, \pi^0)_{\text{decay}}$ and $(\pi^-, \pi^0)_{\text{extra}}$ reactions and the full (π^-, π^0) spectra, respectively. The data are from Table I. Squares and triangles show the zero-degree cross sections divided by $\bar{A} = 3Z + N$ for the $(^3\text{He}, t)$ (Refs. 2–4) and (p, n) (Refs. 5, 6, 8, and 9) reactions, respectively. The data are from Table III. The lines shown are a fit of the data to $A^{-\alpha}$ with $\alpha = 0.59 \pm 0.16$ for $(\pi^-, \pi^0)_{\text{decay}}$, $\alpha = 0.55 \pm 0.14$ for $(\pi^-, \pi^0)_{\text{extra}}$, $\alpha = 0.52 \pm 0.10$ for the full (π^-, π^0) spectra, $\alpha = 0.48 \pm 0.12$ for $(^3\text{He}, t)$, and $\alpha = 0.45 \pm 0.03$ for (p, n) .

TABLE III. Zero-degree laboratory differential cross sections (in mb/sr) to the well-defined delta bump in the (p,n) reaction at 800 MeV and in the ($^3\text{He,t}$) reaction at 2 GeV. $\tilde{A} = N + 3Z$ for these reactions.

	\tilde{A}	$\frac{d\sigma}{d\Omega}$	$\left[\frac{d\sigma}{d\Omega}\right] / \tilde{A}$	Ref.	$\frac{d\sigma}{d\Omega}$	$\left[\frac{d\sigma}{d\Omega}\right] / \tilde{A}$	Ref.
^1H	3	33±4.3	11.0±1.4	6	50±8	17±2.3	4
^2H	4	67±8.7	16.8±2.2	6			
^6Li	12	108±14	9.0±1.2	8			
^7Li	13	121±16	9.3±1.2	8			
C	24	189±19	7.9±0.8	9	45±9	1.87±0.37	3
					40±10	1.67±0.42	2
Al	53	271±38	5.1±0.7	5			
		308±31	5.8±0.6	9			
Ca	80				86±24	1.07±0.30	2
Ti	91.9	372±52	4.0±0.6	5			
^{54}Fe	106				130±26	1.23±0.29	3
					102±31	0.96±0.29	2
Cu	121.5	425±59	3.5±0.5	5			
Y	167				165±33	0.99±0.20	3
^{90}Zr	170				160±45	0.94±0.26	2
W	331.9	696±97	2.1±0.3	5			
Pb	371.2	695±97	1.9±0.3	5			
^{208}Pb	372				129±36	0.35±0.10	2
U	422	768±108	1.8±0.3	5			

added for neutrons and protons.

Absorption of the pion on complex targets may be incorporated by the geometrical model,²⁵

$$d\sigma = d\sigma_0 \tilde{A} A^{-\alpha}.$$

For a black disk, the exponent α is $\frac{4}{3}$.²⁵ Figure 10 shows the pion differential cross sections, divided by \tilde{A} , plotted vs A . The model fits the data at 475 MeV on complex targets quite well if we use $\alpha = 0.55 \pm 0.14$ for the "extra" π^0 and $\alpha = 0.59 \pm 0.16$ for the "decay" π^0 . If all the data (even beyond the fits to the specific peaks) are plotted, the fit has the exponent $\alpha = 0.52 \pm 0.10$. Our kinematic decomposition of the spectra thus has no influence on the mass dependence of the cross sections. The hydrogen point was not included in the fits since no absorption process can occur on this target.

Zero-degree cross sections to the well-defined delta bump in the ($^3\text{He,t}$) reaction at 2 GeV (Refs. 2–4) and in the (p,n) reaction at 800 MeV (Refs. 5, 6, 8 and 9) may similarly be compared to the expression

$$d\sigma = d\sigma_0 (N + 3Z) A^{-\alpha}$$

to match the pion results. We now use $N + 3Z = \tilde{A}$. In the laboratory frame this yields $\alpha = 0.48 \pm 0.12$ for ($^3\text{He,t}$) and $\alpha = 0.45 \pm 0.03$ for (p,n). (The data are given in Table III and plotted in Fig. 10.) All three charge-exchange reactions to nuclear delta production thus scale much the same with the target mass at the angle where the cross section is greatest. For photoabsorption $\alpha = 0$ since the cross section for delta production is constant per nucleon.

In the pion charge-exchange reaction to the isobaric analog state (IAS) (a nonspin mode), Rokni *et al.*²⁶ find this geometrical model gives values for α of 0.93 ± 0.05 at 425 MeV and 0.82 ± 0.01 at 500 MeV. These exponents are strikingly different from that obtained in the present

work to the delta peak at a similar pion energy, showing that the mean free path of the projectile is not the determining factor for the absorption. Rather, the similarity of all exponents, for either longitudinal or transverse excitation of the delta, points to the role of the nuclear form factor for the large momentum transfers. The IAS result is measured at very small momentum transfer.

VI. CONCLUSIONS

For the first time we have looked at delta production in complex nuclei by a pion beam. We have tried to make several comparisons between proton and complex targets. Since the beam energy was not high enough to separate the "extra" and "decay" pions and demonstrate a single clear peak in the spectra, our data are inconclusive as to whether there is a kinematic shift for complex targets. However, one other comparison is possible. In both proton and complex targets, we see a widely spread yield between 100 and 300 MeV as kinematics predict for quasi-free scattering to a delta particle.

Perhaps the most striking feature found in our analysis is the very similar mass dependence of charge-exchange cross sections, divided by the weighted number of participants \tilde{A} , for all three reactions, (π^-, π^0), (p,n), and ($^3\text{He,t}$). Although the data set for the (π^-, π^0) reaction is sparse, the $A^{-1/2}$ dependence of the reduced cross sections is clear. It remains to be understood in detail why both longitudinal and transverse charge-exchange reactions for delta production behave in such similar fashions.

ACKNOWLEDGMENTS

We would like to thank H. Baer for assistance in setting up the experiment and J. D. Bowman for assistance in setting up the sampling grid scintillator. This work was supported in part by the U.S. Department of Energy.

*Present address: P3 MS D-449, Los Alamos National Laboratory, Los Alamos, NM 87545.

- ¹D. Contardo *et al.*, Phys. Lett. **168B**, 331 (1986).
²C. Gaarde, in Proceedings of the Symposium on Delta-Nucleus Dynamics, 1983, edited by T.-S. H. Lee, D. F. Geesaman, and J. P. Schiffer, Argonne National Laboratory Report PHY-83-1-CONF-830588 1983, p. 395.
³C. Ellegaard *et al.*, Phys. Rev. Lett. **50**, 1745 (1983).
⁴C. Ellegaard *et al.*, Phys. Lett. **154B**, 110 (1985).
⁵B. E. Bonner *et al.*, Phys. Rev. C **18**, 1418 (1978).
⁶C. W. Bjork *et al.*, Phys. Lett. **63B**, 31 (1976).
⁷P. J. Riley *et al.*, Phys. Lett. **68B**, 217 (1977).
⁸R. G. Jeppesen, Ph.D. thesis, University of Colorado, 1986 (unpublished).
⁹C. G. Cassapakis *et al.*, Phys. Lett. **63B**, 35 (1976).
¹⁰H. Esbensen and T.-S. H. Lee, Phys. Rev. C **32**, 1966 (1985).
¹¹D. Bachelier *et al.*, Phys. Lett. **172B**, 23 (1986).
¹²G. W. Butler *et al.*, Phys. Rev. C **26**, 1737 (1982).
¹³H. W. Baer *et al.*, Nucl. Instrum. Methods **180**, 445 (1981).
¹⁴J. L. Ullmann *et al.*, Phys. Rev. C **33**, 2092 (1986).
¹⁵J. R. Shepard and E. Rost, Phys. Rev. C **25**, 2660 (1982).
¹⁶J. V. Beaupré *et al.*, Nucl. Phys. **B66**, 93 (1973).
¹⁷R. A. Arndt and L. O. Roper, program SAID (Scattering Analysis Interactive Dialin).
¹⁸S. Jonsson *et al.*, Phys. Rev. C **21**, 306 (1980).
¹⁹R. Cenni and G. Dillon, Nucl. Phys. **A422**, 527 (1984).
²⁰V. F. Dmitriev and T. Suzuki, Nucl. Phys. **A438**, 697 (1985).
²¹M. Ericson, in Lectures Given at the International School of Nuclear Physics, Erice, 1983, 7th course: Mesons, Isobars, Quarks, and Nuclear Excitations, Organisation Européenne pour la Recherche Nucléaire Report TH.3625-CERN.
²²M. G. Olsson and G. B. Yodh, Phys. Rev. **145**, 1309 (1966).
²³J. Ahrens and J. S. O'Connell, Comments Nucl. Part. Phys. **14**, 245 (1985).
²⁴T. Suzuki and M. Kohno, Prog. Theor. Phys. **68**, 690 (1982).
²⁵M. B. Johnson, Phys. Rev. C **22**, 192 (1980).
²⁶S. H. Rokni *et al.*, submitted to Phys. Rev. Lett.